Research Article | Vol. 15, No. 10 / 1 Oct 2024 / Biomedical Optics Express 6010
Biomedical Optics EXPRESS

OCTA-ReVA: an open-source toolbox for comprehensive retinal vessel feature analysis in optical coherence tomography angiography

ALBERT K. DADZIE,[1] DAVID LE,[1] MANSOUR ABTAHI,[1] BEHROUZ EBRAHIMI,[1] TOBILOBA ADEJUMO,[1] TAEYOON SON,[1] MICHAEL J. HEIFERMAN,[2] JENNIFER I. LIM,[2] AND XINCHENG YAO[1,2,*]

[1]*Department of Biomedical Engineering, University of Illinois Chicago, Chicago, IL 60607, USA*
[2]*Department of Ophthalmology and Visual Sciences, University of Illinois Chicago, Chicago, IL 60612, USA*
[*]*xcy@uic.edu*

Abstract: Optical coherence tomography angiography (OCTA) has significantly advanced the study and diagnosis of eye diseases. However, current clinical OCTA systems and software tools lack comprehensive quantitative analysis capabilities, limiting their full clinical utility. This paper introduces the OCTA Retinal Vessel Analyzer (OCTA-ReVA), a versatile open-source platform featuring a user-friendly graphical interface designed for the automated extraction and quantitative analysis of OCTA features. OCTA-ReVA includes traditional established OCTA features based on binary vascular image processing, such as blood vessel density (BVD), foveal avascular zone area (FAZ-A), blood vessel tortuosity (BVT), and blood vessel caliber (BVC). Additionally, it introduces new features based on blood perfusion intensity processing, such as perfusion intensity density (PID), vessel area flux (VAF), and normalized blood flow index (NBFI), which provide deeper insights into retinal perfusion conditions. These additional capabilities are crucial for the early detection and monitoring of retinal diseases. OCTA-ReVA demystifies the intricate task of retinal vasculature quantification, offering a robust tool for researchers and clinicians to objectively evaluate eye diseases and enhance the precision of retinal health assessments.

1. Introduction

Optical coherence tomography angiography (OCTA) is a non-invasive imaging technique that generates volumetric angiography images within seconds. It has become instrumental in the study of retinal vascular pathologies, allowing for detailed assessment of retinal perfusion without the need for contrast agents. OCTA has been extensively explored in the study of eye diseases like diabetic retinopathy (DR) [1–6], glaucoma [7,8], sickle cell retinopathy (SCR) [9–11], age-related macular degeneration (AMD) [12–14] and other diseases. Unlike other imaging modalities such as color fundus photography, scanning laser ophthalmoscopy, and fluorescein angiography, which lack the ability to differentiate individual vascular plexuses due to limited segmentation capabilities, OCTA stands out for its unique capability to discern and differentiate specific plexus layers within the retina. This facilitates a more comprehensive and detailed analysis of retinal microvasculature, allowing researchers and clinicians to precisely investigate and understand alterations in distinct layers associated with various ocular pathologies.

The development of quantitative OCTA features has played a significant role in diagnosing and managing ocular diseases. Quantitative OCTA metrics offer precise evaluations of the retinal blood vessels, enabling consistent, objective assessments of vascular alterations linked to eye disorders. Currently, clinical OCTA devices offer a limited number of quantitative features, including blood vessel density (BVD) and foveal avascular zone area (FAZ-A). While these

#537727 https://doi.org/10.1364/BOE.537727
Journal © 2024 Received 26 Jul 2024; revised 14 Sep 2024; accepted 18 Sep 2024; published 25 Sep 2024

Biomedical Optics EXPRESS

features offer valuable insights into retinal vasculature, it is crucial to recognize that different diseases can manifest unique OCTA changes. This underscores the need for more sophisticated tools enabling comprehensive analysis.

In recent years, several open-source tools have been developed for quantitative OCTA analysis, many of which include user-friendly graphical user interfaces (GUIs). These tools have contributed significantly to the standardization and accessibility of comprehensive OCTA analysis. For instance, Amirmoezzi et al. developed an open-source toolbox for quantitative OCTA analysis [15], focusing on providing measurements of several FAZ metrics. Similarly, Untracht et al. developed the OCTAVA toolbox aimed at standardizing retinal OCTA analysis [16]. While these toolboxes have advanced the field, they mainly focus on binary image processing based OCTA features, such as BVD, blood vessel tortuosity (BVT), blood vessel caliber (BVC), vessel perimeter index (VPI), FAZ contour irregularity (FAZ-CI), FAZ perimeter (FAZ-P), and vessel complexity index (VCI), providing limited features for blood flow perfusion information available in OCTA, which is critical for understanding retinal health and disease progression [17–20].

Recognizing the gap in existing tools, we developed the OCTA Retinal Vessel Analyzer (OCTA-ReVA), an innovative software designed to enhance OCTA data analysis. OCTA-ReVA includes traditional established OCTA features based on binary vascular image processing, such as BVD, BVC, VSD, VPI, BVT, VCI, FAZ-A, FAZ-P, and FAZ-CI. Most importantly, it introduces new features based on blood flow perfusion intensity processing, such as perfusion intensity density (PID), vessel area flux (VAF), and normalized blood flow index (NBFI). These new features provide deeper insights into the perfusion status of retinal tissues, offering critical parameters for early detection and monitoring of various retinal diseases. Recent publications have highlighted how these perfusion intensity processing improve the accuracy of DR staging [4–6].

Recent literature highlights the critical importance of standardizing retinal OCTA to ensure consistency and comparability across studies and clinical practices. Sampson et al. extensively discussed the need for standardized protocols in OCTA imaging, emphasizing that variability in image acquisition and processing can lead to inconsistencies in retinal assessments. Their review underscores the significance of adopting uniform terminology and measurement criteria to enhance the reproducibility of OCTA studies and facilitate multi-center collaborations [20]. Munk et al. also contribute to this discourse by presenting the first survey results aimed at standardizing OCTA nomenclature in retinal vascular diseases. They highlight the consensus among experts regarding the definitions and naming conventions for various OCTA metrics, which is crucial for aligning research outputs with commercial OCTA instruments [21]. Considering these efforts, we have also used standardized terms and definitions for our quantitative OCTA features. Also, we ensured that our definitions for metrics like FAZ-A, FAZ-CI, and BVT were consistent with those proposed in the recent literature. This alignment will facilitate easier comparison with other studies and enhance the clinical relevance of the toolbox.

OCTA-ReVA's comprehensive suite of features, combined with its intuitive GUI, simplifies the analysis process for users with varying levels of technical expertise. This broad spectrum of features facilitates a nuanced examination of retinal vasculature, thereby enhancing the detection, classification, and monitoring of retinal diseases. By integrating sophisticated algorithms for image analysis within a user-friendly platform, OCTA-ReVA aims to support evidence-based clinical decision-making and advance research in ophthalmology.

2. Methods

2.1. Development environment

The OCTA-ReVA toolbox was developed using MATLAB R2022a (MathWorks, Natick, MA, USA). MATLAB's extensive libraries and toolboxes, specifically tailored for image analysis, provided a robust foundation for designing the advanced algorithms necessary for OCTA feature

Biomedical Optics EXPRESS

extraction. The GUI was developed using MATLAB App Designer development environment. The GUI's layout was strategically planned to ensure ease of use, with straightforward navigation, real-time image analysis, result displays, and accessible control elements. This focus on user experience is aimed at democratizing the use of advanced OCTA analysis, making it accessible to clinicians and researchers irrespective of their computational expertise. Figure 1 shows a screenshot of the toolbox.

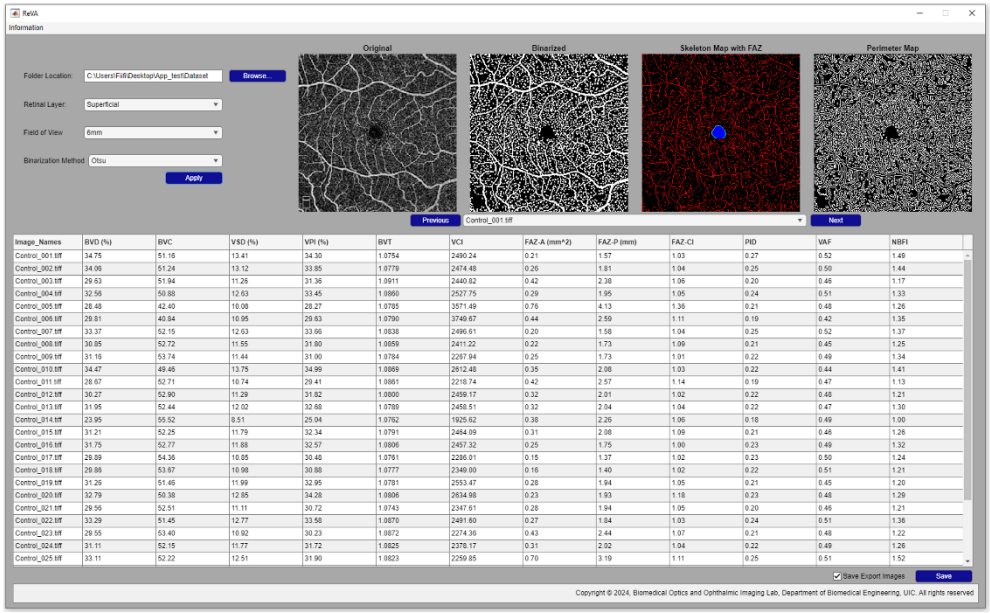

Fig. 1. Screenshot of the OCTA-ReVA toolbox.

2.2. Graphical user interface (GUI)

The OCTA-ReVA toolbox, as shown in Fig. 1, features an intuitive and interactive interface. The design incorporates interactive elements such as buttons and drop-down menus for easy navigation and control. Real-time visualization panels display OCTA images alongside their analysis results, allowing the user to interact with the data directly. The output can be saved locally to the user's personal computer. The toolbox saves both intermediate images used in the calculation of the various metrics and a Microsoft Excel sheet containing the results of the analysis. The intermediate images include binary vessel maps, skeletonized vessel maps, vessel perimeter maps, FAZ masks, and FAZ contour masks. Figure 2 shows representative intermediate images that are saved.

2.3. Quantitative features

The OCTA-ReVA toolbox provides BVD, VSD, FAZ-A, FAZ-P, FAZ-CI, PID, VAF, and NBFI for both superficial and deep layers. Additionally, it offers BVC, VPI, BVT, and VCI for the superficial layer. The calculation and the significance in retinal disease of these features have been comprehensively discussed [5,21,22]. A brief explanation of these features and how they are calculated is given below.

BVD: This feature, also known as vessel density, reflects the portion of the OCTA image occupied by blood vessels. It is pivotal in detecting early phases of different conditions that may

Biomedical Optics EXPRESS

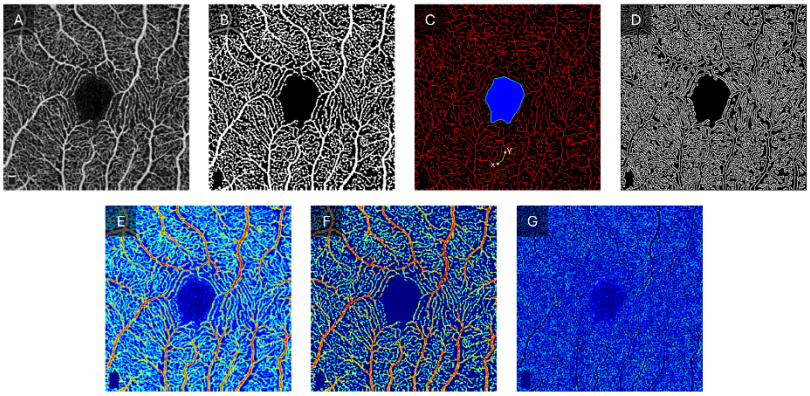

Fig. 2. Intermediates images used in the calculation of the quantitative OCTA features. A) Original OCTA image. B) Binarized vessel map. C) Skeletonized vessel map (red) with FAZ segmented (blue region) and FAZ contour (green outline). One representative vessel branch is highlighted in green with X and Y endpoints identified with yellow dots. D) Vessel perimeter map. E. Original OCTA image with a pseudo-color map. F. OCTA image with the noise removed. G. Background noise removed from the OCTA image.

present with ischemia and dropout zones in the retinal vasculature.

$$BVD = \frac{\sum_{x=1,\,y=1}^{n} A(x,y)}{\sum_{x=1,\,y=1}^{n} I(x,y)} \tag{1}$$

where $A(x, y)$ represents the pixels occupied by the vessels in the binary vessel map (Fig. 2(B)), and $I(x, y)$ represents all the pixels in the OCTA image.

BVC: This feature measures the diameter, or width, of the blood vessels, indicating vascular dilation or constriction associated with various retinopathies.

$$BVC = \frac{\sum_{x=1,\,y=1}^{n} A(x,y)}{\sum_{x=1,\,y=1}^{n} S(x,y)} \tag{2}$$

where $A(x, y)$ represents the pixels occupied by the vessels in the binary vessel map (Fig. 2(B)), and $S(x, y)$ represents the pixels occupied by the vessels in the skeletonized vessel map (Fig. 2(C)).

VSD: This feature is calculated from the skeletonized vessel map. It measures the vascular network's density by reducing vessel thickness to a single pixel, offering insights into vascular architecture.

$$VSD = \frac{\sum_{x=1,\,y=1}^{n} S(x,y)}{\sum_{x=1,\,y=1}^{n} I(x,y)} \tag{3}$$

where $S(x, y)$ represents the pixels occupied by the vessels in the skeletonized vessel map (Fig. 2(C)) and $I(x, y)$ represents all the pixels in the OCTA image.

VPI: This feature measures the ratio between the total perimeter length of blood vessels and their overall area within the OCTA image. This feature is particularly useful for detecting vascular changes indicative of early ischemia or vessel dropout.

$$VPI = \frac{\sum_{x=1,\,y=1}^{n} P(x,y)}{\sum_{x=1,\,y=1}^{n} I(x,y)} \tag{4}$$

where $P(x, y)$ represents the pixels within the vessel perimeters, [the total length of blood vessel outlines (Fig. 2(D))], and $I(x, y)$ represents all the pixels in the OCTA image.

Biomedical Optics EXPRESS

BVT: This feature quantifies the degree of vessel distortion, reflecting blood transport efficiency. Increased tortuosity can signal compromised vessel structure in diseased conditions.

$$BVT = \frac{1}{n}\sum_{i=1}^{n}\left(\frac{\{Geodesic\ distance\ between\ two\ endpoints\ of\ a\ vessel\ branch\ i\}}{\{Euclidean\ distance\ between\ two\ endpoints\ of\ a\ vessel\ branch\ i\}}\right) \quad (5)$$

where i represents the ith vessel branch in the skeletonized vessel map (Fig. 2(C)) and n is the total number of branches. The Euclidean distance represents the straight distance between two endpoints of a vessel branch, while the geodesic distance indicates the total length along the curve between the same endpoints.

VCI: This feature quantifies the complexity and inhomogeneity of the vascular network. Typically, capillary dropout associated with various retinal diseases results in a less complex vasculature.

$$VCI = \frac{\left(\sum_{x=1,\,y=1}^{n} P(x,y)\right)^2}{4\pi\left(\sum_{x=1,\,y=1}^{n} A(x,y)\right)} \quad (6)$$

where $P(x, y)$ represents the pixels within the vessel perimeters (Fig. 2(D)) and $A(x, y)$ represents the pixels occupied by the vessels in the binary vessel map (Fig. 2(B)).

FAZ-A: This feature measures the area of the FAZ, providing insights into the extent of avascular regions in the retina. A larger FAZ area can indicate ischemia or other pathological changes in the retinal vasculature.

$$FAZ - A = \left[Area\ of\ a\ single\ pixel\ (in\ \mu m^2) \times \sum_{x=1,\,y=1}^{n} A(x,y)\right] \quad (7)$$

where $A(x, y)$ represents the pixels occupied by the segmented FAZ region (blue region in Fig. 2(C)).

FAZ-P: This feature measures the perimeter of the FAZ, reflecting the boundary length of the FAZ. Changes in FAZ-P can indicate alterations in the retinal vascular architecture.

$$FAZ - P = \left[Length\ of\ a\ single\ pixel\ (in\ \mu m) \times \sum_{x=1,\,y=1}^{n} P(x,y)\right] \quad (8)$$

where $P(x, y)$ corresponds to the pixels of the perimeter of the FAZ (green demarcation in Fig. 2(C)).

FAZ-CI: This feature measures the irregularity of the FAZ contour, providing a metric for the complexity and deviations in the shape of the FAZ. Higher contour irregularity indicates more pronounced pathological changes.

$$FAZ - CI = \frac{\sum_{x=1,\,y=1}^{n1} P(x,y)}{\sum_{x=1,y=1}^{n2} R(x,y)} \quad (9)$$

where $P(x, y)$ represents the pixels forming the perimeter of the FAZ (indicated by the green demarcation in Fig. 2(C)), and $R(x, y)$ represents the pixels forming the perimeter of a reference circle with an area identical to the segmented FAZ. $n1$ denotes the total number of pixels along the FAZ perimeter while $n2$ denotes the total number of pixels along the perimeter of the reference circle.

Biomedical Optics EXPRESS

PID: This feature provides a metric to quantify blood flow in OCTA images without the need for binarization. It is calculated directly from the OCTA image without any preprocessing.

$$PID = \mu(Original\ OCTA\ Image) \tag{10}$$

VAF: This feature quantifies blood flow from areas of perfusion in the OCTA image. The binary map is used to select areas of perfusion in the OCTA image.

$$VAF = \frac{\sum_{x=1,\ y=1}^{n} F_I(x,y)}{\sum_{x=1,y=1}^{n} F(x,y)} \tag{11}$$

where $F_I(x, y)$ represents the pixel intensities of the area covered by blood vessels and $F(x, y)$ represents all the vessels corresponding to blood vessels in the OCTA image.

NBFI: This feature provides a measure of blood flow which is normalized for variations in image acquisition and processing.

$$NBFI = \frac{\mu(Noiseless\ OCTA\ Image)}{\sigma(Noise\ Map)} \tag{12}$$

2.4. Binary image processing

Binary image processing is a crucial step in the extraction of OCTA features, except for PID. This process converts the OCTA images into binary format, where blood vessels are depicted as white pixels (value = 1) and the background as black pixels (value = 0). This conversion isolates vascular structures from the background, facilitating accurate measurement of quantitative features. To enhance vessel detection, the Frangi "vesselness" filter was first applied to the enface OCTA images. Subsequently, a threshold value is set to classify each pixel in the OCTA image as either part of a vessel (white) or part of the background (black). Selecting an appropriate threshold is critical for accurate binarization, as it directly affects the detection of vessels and, hence, the calculation of OCTA features.

The OCTA-ReVA toolbox is equipped with five different methods to determine the threshold for binarization. These include the Otsu method, fixed thresholding, mean thresholding, median thresholding, and the 3-sigma method. The vessel maps generated using the various binarization techniques are shown in Fig. 3. The inclusion of these diverse thresholding techniques within the toolbox aligns with the findings from the study by Rabiolo et al., which showed significant variability in BVD calculation across different thresholding methods in OCTA images [23]. OCTA images vary significantly based on the patient demographics, disease state, and acquisition settings, with different segmentation methods optimized for various image characteristics. OCTA-ReVA accommodates a wide range of datasets by providing multiple segmentation options, ensuring accurate segmentation across diverse conditions. Since no single method works best for all image types, such as Otsu's method being good for high-contrast images but not for uneven illumination, offering multiple methods improves the accuracy and reliability of metrics. Additionally, multiple methods facilitate comparison and validation within the same toolbox, allowing users to determine the most consistent and accurate results for their datasets. Brief explanations of the available thresholding algorithms are provided below.

Otsu method: This approach selects a threshold that minimizes the within-class variance of the black and white pixels or, equivalently, maximizes the between-class variance. It is particularly effective for images with a clear bimodal distribution of pixel intensities. This method is highly suitable for OCTA images with distinct contrast between the vessels and the background.

Fixed thresholding: A predefined intensity value is used as the threshold for binarization. Pixels above this value are converted to white and those below to black. While this approach is straightforward, it requires prior knowledge and/or experimentation to identify the optimal

Biomedical Optics EXPRESS

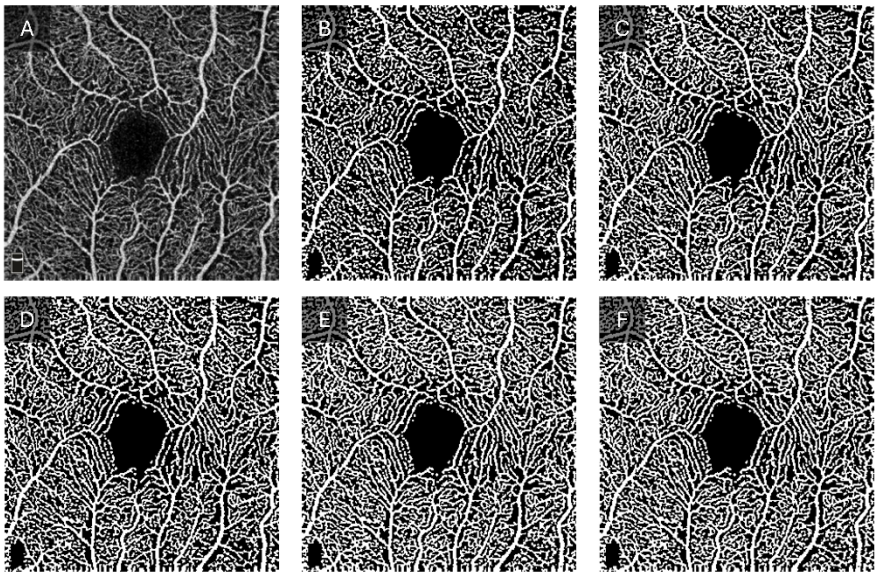

Fig. 3. Binary vessels maps generated using various binarization techniques. A) Original OCTA image. B) Otsu method. C) Fixed thresholding with a threshold value of 0.3. D) Mean thresholding. E) Median thresholding. F) 3-sigma method.

threshold value. It works best for datasets with consistent image quality and contrast levels. In the OCTA-ReVA toolbox, the value input by the user is used as the threshold for all the images loaded into the toolbox.

Mean thresholding: This approach calculates the average pixel intensity of the OCTA image and uses this value as the threshold. Unlike the fixed method, the mean of each image is calculated as the threshold to be used for that image.

Median thresholding: This approach involves using the median pixel intensity value of the image as the threshold. This technique is less sensitive to outliers than mean thresholding, providing a robust thresholding solution for images with uneven illumination or contrast. Like the mean thresholding, the median intensity value of each image is calculated and used as the threshold for that particular image.

3-sigma method: This approach sets the threshold at three standard deviations from the mean intensity value. This is effective for images where vessels and background intensities are well separated by intensity values. In OCTA images, the intensities of blood vessels are comparatively high compared to the background and noise. For the 3-sigma approach used in the OCTA-ReVA, the mean value plus three standard deviations from the mean of 40% of the total pixels with the lowest intensities are calculated from each OCTA image. Several studies have reported BVD to be in the range of 20% - 60% [24–27], and thus, 40% of the pixels with the lowest intensities reliably reflect the background and noise in the OCTA image.

2.5. OCTA dataset and statistical analysis

OCTA images from 20 control subjects were collected and used to validate the OCTA-ReVA toolbox. The Angiovue spectral domain OCT (Optovue, Fremont, CA, USA) was used to obtain 6 mm $\times$ 6 mm macular scans from each subject. OCTA enface images of the superficial vascular plexus were extracted using the built-in ReVue software (version 2018.1.0.43). The quantitative features were calculated from these images using various binarization techniques. We then compared the results from the different binarization techniques.

Biomedical Optics EXPRESS

To assess the repeatability of the quantitative feature analysis, three repeated OCTA measurements of each eye were taken from a subset of four control subjects, and the coefficient of variation (CV) was used to quantify the relative variability across repeated measurements. The CV of each quantitative feature was calculated using the formula:

$$CV = \frac{\sigma}{\mu} \times 100 \tag{13}$$

where σ and μ stand for the standard deviation and mean of the quantitative feature. A CV below 10% is considered very good, 10–20% is considered good, 20–30% is acceptable, and above 30% is unacceptable. Additionally, we performed the Friedman test to determine if there were any statistically significant differences between the repeated measurements.

We also used the OCTA-ReVA toolbox to analyze OCTA images from a cohort of patients with different stages of DR, including diabetics with no clinical signs of retinopathy (NoDR), mild non-proliferative DR (NPDR), moderate NPDR, and severe NPDR. The images were 6 mm x 6 mm from the superficial and deep plexuses. The Otsu binarization technique was used for all the analyses.

Statistical analysis was performed using R Software, version 4.3.2 (R Core Team, Vienna, Austria). The Shapiro-Wilk test was first used to check for the normality of the quantitative features using the different binarization techniques. Comparisons between the different binarization techniques were performed using one-way analysis of variance (ANOVA) for normally distributed data and the Kruskal-Wallis test for non-normally distributed data. Also, the Spearman correlation test was used to determine the correlation of the quantitative features using different binarization techniques. Comparisons between the quantitative features between the controls and the DR patients were done using the ANOVA test for normally distributed data, and the Kruskal-Wallis test was used for non-normally distributed data. A P value <0.05 was considered statistically significant.

3. Results

A total of 30 eyes from 20 healthy control subjects were used to validate the OCTA-ReVA toolbox. Additionally, the toolbox was used to study 21 eyes from 15 NoDR subjects, 26 eyes from 22 mild NPDR patients, 36 eyes from 22 moderate NPDR patients, and 12 eyes from 7 severe NPDR. A summary of the characteristics of the subjects is provided in Table 1.

Table 1. Demographics of Subjects

	Control	NoDR	Mild	Moderate	Severe
No. of subjects	20	15	22	22	7
Gender					
Male	13	5	9	8	3
Female	7	10	13	14	4
Age (year)	53.68 ± 14.59	57.29 ± 10.74	61.19 ± 11.27	62.14 ± 9.94	62.92 ± 4.89
Age Range	37 - 80	40 - 80	24 - 78	41 - 86	57 - 74
No. of Images	30	21	26	36	12
Eye					
Right	14	10	11	18	6
Left	16	11	15	18	6

The comparative analysis of the quantitative features across the various binarization techniques is shown in Table 2. Significant variability was observed across the different binarization

Biomedical Optics EXPRESS

techniques. The results show that the choice of binarization technique has a significant impact on most quantitative OCTA features ($p < 0.0001$). The Otsu method generally yielded more conservative values, suggesting a stricter criterion for distinguishing vessels from the background.

Table 2. Comparison of quantitative OCTA features using different binarization techniques

Quantitative Feature	Otsu	Fixed	Mean	Median	3-Sigma	P-Value
BVD (%)	30.12 ± 3.10	31.92 ± 3.95	39.05 ± 1.81	42.99 ± 1.21	41.47 ± 0.83	**<.0001**[b]
BVC (μm)	45.81 ± 5.47	44.86 ± 5.32	40.78 ± 4.80	39.01 ± 4.66	39.66 ± 4.85	**<.0001**[b]
VSD (%)	11.03 ± 1.49	11.97 ± 2.01	16.02 ± 1.80	18.42 ± 0.92	17.48 ± 0.63	**<.0001**[b]
VPI (%)	30.17 ± 2.97	31.47 ± 3.42	35.65 ± 1.37	36.86 ± 0.92	36.48 ± 0.79	**<.0001**[b]
BVT	1.079 ± 0.005	1.082 ± 0.005	1.084 ± 0.004	1.084 ± 0.003	1.084 ± 0.004	**<.0001**[a]
VCI ($x10^2$)	32.27 ± 7.73	33.03 ± 7.53	34.77 ± 7.56	33.78 ± 7.41	34.29 ± 7.45	0.1711[b]
VAF	0.50 ± 0.02	0.48 ± 0.01	0.40 ± 0.03	0.37 ± 0.03	0.38 ± 0.03	**<.0001**[b]
NBFI	1.30 ± 0.14	1.46 ± 0.24	2.38 ± 0.06	3.19 ± 0.18	2.87 ± 0.30	**<.0001**[b]

[a]Multiple group comparisons performed using one-way ANOVA test.
[b]Multiple group comparisons performed using Kruskal-Wallis test.

The result from the correlation analysis is shown in Fig. 4. Despite the differences in the absolute values obtained using different binarization techniques, the correlation matrices demonstrate that these values are all positively correlated. This positive correlation suggests that while the magnitudes of the measurements may vary, the trends and relative changes in the measurements are consistent across the different techniques. For most features, the correlation coefficients are close to 1, indicating a strong positive correlation. However, features such as BVT, VAF, and NBFI have some coefficients being lower, indicating moderate to weak positive correlations. This suggests that these features are more sensitive to the choice of binarization.

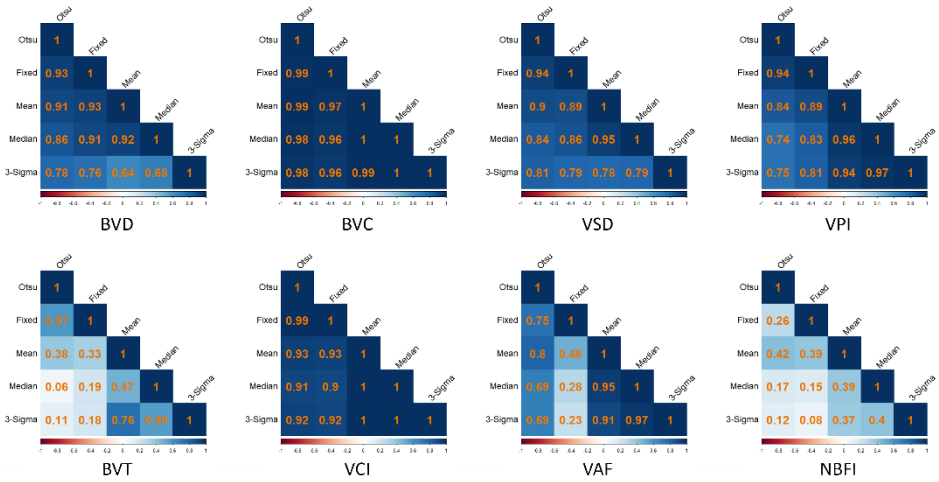

Fig. 4. Correlation matrix showing the relationship between the various binarization techniques in the calculation of the quantitative OCTA features. The colormap represents correlation coefficients, with darker colors indicating higher correlation and lighter colors indicating lower correlation. Red indicates negative correlation, and blue indicates positive correlation.

The results of the repeatability analysis are shown in Table 3. The mean CV for all quantitative features was below 10%, indicating a high level of repeatability and consistency across the

Biomedical Optics EXPRESS

repeated measurements. Additionally, the p-values from the Friedman test for all quantitative features were above 0.05, indicating no statistically significant differences between the repeated measurements. This further supports the consistency and robustness of the OCTA-ReVA toolbox.

Table 3. Repeatability Analysis of Quantitative OCTA Features

Quantitative Feature	Coefficient of Variation (%)	Time 1	Time 2	Time 3	P-Value
BVD	4.46 ± 3.46	31.04 ± 2.69	30.27 ± 2.00	31.01 ± 1.87	0.4169
BVC	2.25 ± 1.31	26.65 ± 1.15	27.06 ± 0.68	27.00 ± 1.08	0.4169
VSD	6.52 ± 4.53	11.55 ± 1.38	11.06 ± 0.98	11.37 ± 1.09	0.1969
VPI	3.97 ± 2.98	30.04 ± 2.30	29.58 ± 1.35	29.87 ± 1.97	0.6065
BVT	0.30 ± 0.22	1.081 ± 0.004	1.081 ± 0.006	1.084 ± 0.008	0.0724
VCI	3.71 ± 2.72	21.38 ± 1.48	21.27 ± 0.07	21.18 ± 16.43	0.8825
FAZ-A	7.27 ± 5.15	0.41 ± 0.08	0.43 ± 0.09	0.41 ± 0.10	0.7480
FAZ-P	5.90 ± 3.58	2.58 ± 0.19	2.66 ± 0.32	2.53 ± 0.23	0.6873
FAZ-CI	3.60 ± 1.70	1.16 ± 0.08	1.16 ± 0.08	1.14 ± 0.07	0.7979
PID	4.82 ± 3.41	0.23 ± 0.01	0.23 ± 0.02	0.24 ± 0.02	0.6977
VAF	1.74 ± 1.24	0.51 ± 0.01	0.51 ± 0.02	0.52 ± 0.02	0.7640
NBFI	5.70 ± 4.06	1.48 ± 0.16	1.42 ± 0.14	1.49 ± 0.12	0.3031

Table 4. Comparative analysis of the quantitative OCTA features in DR patients (Superficial Layer)

Quantitative Feature	Control	NoDR	Mild	Moderate	Severe	P-Value
BVD (%)	30.12 ± 3.10	29.88 ± 3.58	28.76 ± 2.80	26.99 ± 2.86	25.66 ± 2.30	**<.0001**[a]
BVC (μm)	45.81 ± 5.47	42.19 ± 2.90	47.64 ± 5.72	42.41 ± 1.34	42.39 ± 0.94	**0.0148**[b]
VSD (%)	11.03 ± 1.49	10.84 ± 1.66	10.55 ± 1.33	9.57 ± 1.20	9.10 ± 0.96	**<.0001**[a]
VPI (%)	30.17 ± 2.97	29.68 ± 3.55	28.76 ± 2.77	26.42 ± 2.95	24.96 ± 2.54	**<.0001**[b]
BVT	1.079 ± 0.005	1.080 ± 0.005	1.078 ± 0.005	1.078 ± 0.004	1.077 ± 0.005	0.5600[b]
VCI (x10^2)	32.27 ± 7.73	36.79 ± 5.64	28.16 ± 2.77	32.96 ± 4.08	30.92 ± 3.61	**0.0003**[b]
FAZ-A (mm2)	0.48 ± 0.23	0.77 ± 0.49	0.63 ± 0.30	0.86 ± 0.74	1.10 ± 0.70	**0.0019**[b]
FAZ-P (mm)	2.65 ± 0.69	3.38 ± 1.08	3.21 ± 0.97	3.87 ± 1.71	5.29 ± 2.21	**<.0001**[b]
FAZ-CI	1.11 ± 0.06	1.13 ± 0.07	1.18 ± 0.11	1.24 ± 0.14	1.46 ± 0.3	**<.0001**[b]
PID	0.22 ± 0.02	0.22 ± 0.03	0.21 ± 0.02	0.20 ± 0.02	0.19 ± 0.02	**0.0001**[b]
VAF	0.50 ± 0.02	0.49 ± 0.03	0.50 ± 0.03	0.48 ± 0.03	0.49 ± 0.04	0.1514[b]
NBFI	1.30 ± 0.14	1.32 ± 0.16	1.27 ± 0.12	1.25 ± 0.11	1.24 ± 0.09	0.2710[a]

[a]Multiple group comparisons performed using one-way ANOVA test.
[b]Multiple group comparisons performed using Kruskal-Wallis test.

Tables 4 and 5 present the comparative analysis of various quantitative OCTA features across different stages of DR in the superficial and deep retinal layers, respectively. Across both the superficial and deep layers, a consistent trend of decreasing BVD and VSD was observed with the progression of DR, indicating a significant loss of vascular structures as the disease advances, which is a hallmark of DR. BVC, however, shows an initial increase in the early stages and subsequent decline as the disease advances. The results show that BVT remained relatively stable, indicating that vessel curvature does not significantly change with DR progression. The FAZ metrics showed significant increases with worsening DR, reflecting the enlargement and irregularity of the FAZ. Perfusion-related features, including PID, VAF, and NBFI, showed varied

Biomedical Optics EXPRESS

patterns between the layers, with significant decreases in NBFI, particularly in the deep layer, indicating impaired blood flow as DR progresses.

Table 5. Comparative analysis of the quantitative OCTA features in DR patients (Deep)

Quantitative Feature	Control	NoDR	Mild	Moderate	Severe	P-Value
BVD (%)	37.24 ± 4.18	35.57 ± 4.58	33.19 ± 4.62	30.63 ± 4.17	29.72 ± 3.10	**<.0001**[b]
VSD (%)	15.73 ± 1.49	14.56 ± 2.83	13.23 ± 2.74	11.68 ± 2.15	11.10 ± 1.57	**<.0001**[b]
FAZ-A (mm2)	0.28 ± 0.09	0.48 ± 0.45	0.41 ± 0.17	0.47 ± 0.29	0.45 ± 0.19	**0.0006**[b]
FAZ-P (mm)	1.86 ± 0.34	2.49 ± 1.19	2.37 ± 0.68	2.63 ± 0.91	2.60 ± 0.66	**<.0001**[b]
FAZ-CI	1.03 ± 0.02	1.08 ± 0.08	1.08 ± 0.08	1.13 ± 0.11	1.14 ± 0.05	**<.0001**[b]
PID	0.24 ± 0.03	0.24 ± 0.04	0.21 ± 0.03	0.20 ± 0.03	0.20 ± 0.03	**<.0001**[b]
VAF	0.46 ± 0.03	0.46 ± 0.05	0.44 ± 0.03	0.45 ± 0.03	0.45 ± 0.03	**0.0464**[b]
NBFI	1.78 ± 0.27	1.66 ± 0.32	1.52 ± 0.33	1.41 ± 0.24	1.32 ± 0.15	**<.0001**[a]

[a]Multiple group comparisons performed using one-way ANOVA
[b]Multiple group comparisons performed using Kruskal-Wallis test.

4. Discussion

The development and application of the OCTA-ReVA toolbox represents a pivotal advancement in OCTA analysis. This toolbox, designed with a focus on user-friendliness and comprehensive quantitative analysis, has the potential to transcend the limitations of existing OCTA analytical tools. Unlike current FDA-approved OCTA devices that offer automated calculations for a limited set of features, the OCTA-ReVA enables the calculation of an extended range of quantitative features, including BVD, BVC, VSD, VPI, BVT, VCI, FAZ-A, FAZ-P, FAZ-CI, PID, VAF, and NBFI. This broad spectrum of features facilitates a nuanced examination of retinal vasculature, thereby enhancing the detection, classification, and monitoring of retinal diseases.

Considering the work by Rabiolo et al. [16], the OCTA-ReVA toolbox includes five binarization methods. The significant differences between these techniques align with Rabiolo et al.'s findings, reaffirming that the choice of method can greatly influence the quantitative features extracted from OCTA data. Despite these differences, our analysis revealed a consistent pattern across the methods, which suggests that while the numerical values may differ, the relative differences within the dataset remain stable. In practical terms, this means that while individual values should not be directly compared across different techniques, the overall conclusions drawn from the data analysis are likely to be consistent, provided the same method is used consistently throughout a study. By providing multiple binarization options, the OCTA-ReVA toolbox allows users to select the most appropriate method based on their specific dataset and clinical requirements while still ensuring reliable comparative results. This flexibility and consistency in trends underscore the utility of the toolbox in diverse research and clinical settings.

BVD is probably the most popular quantitative OCTA metric, and it has been used to study several retinal diseases, including DR, AMD, and SCR. However, the pathophysiology of certain diseases suggests that other features than BVD can be more sensitive for detection and classification. For example, in the study by Alam et al., they found that BVT was more sensitive in staging SCR compared to BVD, which was more sensitive in staging DR [28]. This finding is corroborated by the results presented in Table 4, where BVD showed significant differences across the stages of DR, indicating its utility in detecting disease progression. In contrast, BVT remained fairly consistent as DR progressed, suggesting that while BVD is a robust marker for DR, BVT might offer better sensitivity for other diseases like SCR, where vessel tortuosity is more indicative of pathological changes.

Biomedical Optics EXPRESS

Recent studies have shown that perfusion intensity metrics can offer even greater sensitivity for detecting early DR. For instance, Dadzie et al. demonstrated that NBFI is a more sensitive biomarker for detecting early DR compared to BVD, highlighting the importance of these additional metrics in disease diagnosis [4]. Similarly, studies by Abtahi et al. have shown that the inclusion of perfusion intensity metrics improves the classification of DR stages, reinforcing the clinical value of these features [5,6]. This comprehensive analysis is crucial for capturing the multifaceted nature of retinal pathologies, where different diseases may impact the retinal vasculature in unique ways that are best detected by specific metrics.

This emphasizes the need for multiple quantitative OCTA features in the analysis and study of retinal diseases. This comprehensive analysis is crucial for capturing the multifaceted nature of retinal pathologies, where different diseases may impact the retinal vasculature in unique ways that are best detected by specific metrics. The efficacy of BVD in staging DR underscores its relevance in conditions characterized by vascular dropout and ischemia, where vessel density reduction is a hallmark. Conversely, the superior sensitivity of BVT in staging SCR aligns with the disease's pathophysiology, where sickle-shaped blood cells lead to the development of tortuous and dilated vessels. Additionally, combining OCTA metrics can significantly enhance disease detection and classification.

The capability of the OCTA-ReVA toolbox to analyze both the superficial and deep layers of the retina is a significant advancement in the field of retinal imaging and diagnostics. This feature is crucial as different layers can exhibit distinct pathological changes that are essential for accurate diagnosis and effective monitoring of retinal diseases. Several studies have reported that retinal diseases such as DR affect the superficial and deep layers of the retina differently [29–31]. The comparative analysis of the quantitative OCTA features in DR patients, as shown in Tables 4 and 5, indicates that NBFI in the superficial layer does not change significantly as DR progresses, whereas it shows a significant difference in the deep layer. Similar findings have been reported in other studies [32,33].

The combination of several quantitative OCTA features from different retinal layers provides a comprehensive understanding of the pathophysiology of diseases. For instance, as shown in Tables 4 and 5, BVD and VSD significantly decrease in both the superficial and deep layers as DR progresses, indicating a general loss of vascular density. However, other features like BVC provide additional context. Initially, there is a decline in BVC during the very early stages, followed by an increase in the mild stage of the disease. This could be interpreted in the context of the pathophysiological changes that occur during the development and progression of DR. The early microvascular changes due to DR include capillary basement membrane thickening and loss of pericytes, which can lead to decreased vessel caliber [34–36]. As DR progresses and capillary dropout becomes more pronounced, the retinal vessels dilate in response to retinal ischemia and hypoxia to maintain adequate perfusion to meet the metabolic demands of the retina. However, as DR advances further into more severe stages, the vessel caliber begins to decline again after the initial increase. This decline is as a result of the cumulative effects of chronic retinal ischemia and extensive capillary loss, which overwhelm the compensatory mechanisms of vasodilation. The continued damage to the retinal vasculature leads to a reduction in the number of functional capillaries and a subsequent drop in perfusion intensity, which is shown by metrics such as VAF and NBFI.

These observed changes in OCTA metrics for DR highlight the need for sophisticated tools for studying retinal diseases. The OCTA-ReVA toolbox's comprehensive analysis is crucial for understanding the diverse vascular changes across different retinal diseases, including glaucoma, AMD, and SCR. Each disease affects the retinal vasculature in unique ways, necessitating a tool capable of capturing and quantifying these changes. The OCTA-ReVA toolbox will enable clinicians and researchers to assess multiple quantitative OCTA metrics simultaneously, providing a holistic view of the retinal vascular network. Furthermore, the toolbox's user-friendly GUI

Biomedical Optics EXPRESS

will make advanced OCTA analysis accessible to a wide range of users. This approach not only facilitates research in ophthalmology but also supports clinicians with varying degrees of computational expertise in incorporating quantitative OCTA analysis into their practice.

Looking forward, the potential for OCTA-ReVA extends beyond its current capabilities. Future developments could include the integration of artificial intelligence to automate feature detection and classification, enhancing the toolbox's utility in large-scale studies and clinical settings. Future additions will include automatically segmenting arteries and veins in OCTA images for differential artery-vein analysis. Furthermore, the toolbox will support analysis in different regions of the retina, such as the fovea, parafovea, and perifovea, as well as specific quadrants like superior, inferior, nasal, and temporal regions. While this study was limited to images from a single OCTA device, future work will focus on validating the software across multiple platforms to ensure broader applicability. By continuously evolving, the OCTA-ReVA toolbox aims to remain at the forefront of OCTA analysis, providing invaluable support to both clinical and research communities in ophthalmology.

5. Conclusion

The OCTA-ReVA toolbox represents a significant step forward in the analysis of OCTA data, offering an accessible, comprehensive, and nuanced examination of the retinal vasculature. By facilitating detailed assessments of vascular changes associated with a variety of ocular pathologies, OCTA-ReVA supports the advancement of research in ophthalmology and the improvement of clinical decision-making. Additionally, the inclusion of blood flow perfusion intensity features enriches the analysis by providing insights into both structural and functional aspects of the retinal vasculature. This comprehensive approach enhances our understanding of ocular diseases and their progression, contributing valuable information to the field.

Funding. Richard and Loan Hill Department of Biomedical Engineering, University of Illinois at Chicago; Research to Prevent Blindness; National Eye Institute (P30 EY001792, R01 EY023522, R01 EY029673, R01 EY030101, R01 EY030842).

Disclosures. The authors declare no conflicts of interest.

Data availability. The OCTA-ReVA toolbox is publicly available [37]. All data supporting the findings and conclusions presented in this manuscript are included within the manuscript. Additional data may be made available upon reasonable request to the authors.

References

1. B. Ebrahimi, D. Le, M. Abtahi, *et al.*, "Optimizing the OCTA layer fusion option for deep learning classification of diabetic retinopathy," Biomed. Opt. Express **14**(9), 4713–4724 (2023).
2. D. Le, A. Dadzie, T. Son, *et al.*, "Comparative analysis of OCT and OCT angiography characteristics in early diabetic retinopathy," Retina **43**(6), 992–998 (2023).
3. M. Alam, D. Le, J. I. Lim, *et al.*, "Vascular complexity analysis in OCT angiography of diabetic retinopathy," Retina **41**(3), 538–545 (2021).
4. A. K. Dadzie, D. Le, M. Abtahi, *et al.*, "Normalized blood flow index in optical coherence tomography angiography provides a sensitive biomarker of early diabetic retinopathy," Trans. Vis. Sci. Tech. **12**(4), 3 (2023).
5. M. Abtahi, D. Le, B. Ebrahimi, *et al.*, "Differential artery-vein analysis improves the OCTA classification of diabetic retinopathy," Biomed. Opt. Express **15**(6), 3889–3899 (2024).
6. M. Abtahi, D. Le, B. Ebrahimi, *et al.*, "Differential capillary and large vessel analysis improves OCTA classification of diabetic retinopathy," Invest. Ophthalmol. Vis. Sci. **65**(10), 20 (2024).
7. C. Li, L. Tan, X. Xu, *et al.*, "Changes of optic disc and macular vessel perfusion density in primary angle closure glaucoma: a quantitative study using optical coherence tomography angiograph," Ophthalmic Res. **66**(1), 1245–1253 (2023).
8. P. Lu, H. Xiao, C. Liang, *et al.*, "Quantitative analysis of microvasculature in macular and peripapillary regions in early primary open-angle glaucoma," Curr. Eye Res. **45**(5), 629–635 (2020).
9. M. Alam, J. I. Lim, D. Toslak, *et al.*, "Differential artery-vein analysis improves the performance of OCTA staging of sickle cell retinopathy," Trans. Vis. Sci. Tech. **8**(2), 3 (2019).
10. M. Alam, D. Thapa, J. I. Lim, *et al.*, "Computer-aided classification of sickle cell retinopathy using quantitative features in optical coherence tomography angiography," Biomed. Opt. Express **8**(9), 4206–4216 (2017).

Biomedical Optics EXPRESS

11. M. Alam, D. Thapa, J. I. Lim, *et al.*, "Quantitative characteristics of sickle cell retinopathy in optical coherence tomography angiography," Biomed. Opt. Express **8**(3), 1741–1753 (2017).
12. R. Serra, F. Coscas, A. Pinna, *et al.*, "Quantitative optical coherence tomography angiography features of inactive macular neovascularization in age-related macular degeneration," Retina **41**(1), 93–102 (2021).
13. S. Ozcaliskan, O. Artunay, S. Balci, *et al.*, "Quantitative analysis of inner retinal structural and microvascular alterations in intermediate age-related macular degeneration: A swept-source OCT angiography study," Photodiagn. Photodyn. Ther. **32**, 102030 (2020).
14. S. T. Garrity, N. A. Iafe, N. Phasukkijwatana, *et al.*, "Quantitative analysis of three distinct retinal capillary plexuses in healthy eyes using optical coherence tomography angiography," Invest. Ophthalmol. Vis. Sci. **58**(12), 5548–5555 (2017).
15. Y. Amirmoezzi, M. Ghofrani-Jahromi, H. Parsaei, *et al.*, "An open-source image analysis toolbox for quantitative retinal optical coherence tomography angiography," J Biomed Phys Eng **14**(1), 31–42 (2023).
16. G. R. Untracht, M. S. Durkee, M. Zhao, *et al.*, "Towards standardising retinal OCT angiography image analysis with open-source toolbox OCTAVA," Sci. Rep. **14**(1), 5979 (2024).
17. F. Abdolahi, X. Zhou, B. S. Ashimatey, *et al.*, "Optical coherence tomography angiography-derived flux as a measure of physiological changes in retinal capillary blood flow," Trans. Vis. Sci. Tech. **10**(9), 5 (2021).
18. W. J. Choi, W. Qin, C. L. Chen, *et al.*, "Characterizing relationship between optical microangiography signals and capillary flow using microfluidic channels," Biomed. Opt. Express **7**(7), 2709–2728 (2016).
19. S. Kushner-Lenhoff, Y. D. Li, Q. Q. Zhang, *et al.*, "OCTA derived vessel skeleton density versus flux and their associations with systemic determinants of health," Invest. Ophthalmol. Visual Sci. **63**(2), 19 (2022).
20. J. P. Su, R. Chandwani, S. S. Gao, *et al.*, "Calibration of optical coherence tomography angiography with a microfluidic chip," J. Biomed. Opt. **21**(08), 1 (2016).
21. X. Yao, M. N. Alam, D. Le, *et al.*, "Quantitative optical coherence tomography angiography: a review," Exp. Biol. Med. **245**(4), 301–312 (2020).
22. Z. Chu, J. Lin, C. Gao, *et al.*, "Quantitative assessment of the retinal microvasculature using optical coherence tomography angiography," J. Biomed. Opt. **21**(6), 066008 (2016).
23. A. Rabiolo, F. Gelormini, R. Sacconi, *et al.*, "Comparison of methods to quantify macular and peripapillary vessel density in optical coherence tomography angiography," PLoS One **13**(10), e0205773 (2018).
24. M. Alam, Y. Zhang, J. I. Lim, *et al.*, "Quantitative optical coherence tomography angiography features for objective classification and staging of diabetic retinopathy," Retina **40**(2), 322–332 (2020).
25. D. Le, M. Alam, B. A. Miao, *et al.*, "Fully automated geometric feature analysis in optical coherence tomography angiography for objective classification of diabetic retinopathy," Biomed. Opt. Express **10**(5), 2493–2503 (2019).
26. R. Mastropasqua, L. Toto, A. Mastropasqua, *et al.*, "Foveal avascular zone area and parafoveal vessel density measurements in different stages of diabetic retinopathy by optical coherence tomography angiography," Int. J. Ophthalmol. **10**, 1545–1551 (2017).
27. H. Safi, P. Anvari, D. Naseri, *et al.*, "Quantitative analysis of optical coherence tomography angiography metrics in diabetic retinopathy," Ophthalmol. Eye Dis. **12**, 251584141989745 (2020).
28. M. Alam, D. Le, J. I. Lim, *et al.*, "Supervised machine learning based multi-task artificial intelligence classification of retinopathies," J. Clin. Med. **8**(6), 872 (2019).
29. C. Lavia, A. Couturier, A. Erginay, *et al.*, "Reduced vessel density in the superficial and deep plexuses in diabetic retinopathy is associated with structural changes in corresponding retinal layers," PLoS One **14**(7), e0219164 (2019).
30. G. Dimitrova and E. Chihara, "Implication of deep-vascular-layer alteration detected by optical coherence tomography angiography for the pathogenesis of diabetic retinopathy," Ophthalmologica **241**(4), 179–182 (2019).
31. Q. Chen, Q. Ma, C. Wu, *et al.*, "Macular vascular fractal dimension in the deep capillary layer as an early indicator of microvascular loss for retinopathy in type 2 diabetic patients," Invest. Ophthalmol. Visual Sci. **58**(9), 3785–3794 (2017).
32. N. R. Harris, W. Leskova, G. Kaur, *et al.*, "Blood flow distribution and the endothelial surface layer in the diabetic retina," Biorheology **56**(2-3), 181–189 (2019).
33. P. L. Nesper, P. K. Roberts, A. C. Onishi, *et al.*, "Quantifying microvascular abnormalities with increasing severity of diabetic retinopathy using optical coherence tomography angiography," Invest. Ophthalmol. Visual Sci. **58**(6), BIO307 (2017).
34. E. Beltramo and M. Porta, "Pericyte loss in diabetic retinopathy: mechanisms and consequences," Curr. Med. Chem. **20**(26), 3218–3225 (2013).
35. S. Roy and D. Kim, "Retinal capillary basement membrane thickening: role in the pathogenesis of diabetic retinopathy," Prog. Retinal Eye Res. **82**, 100903 (2021).
36. J. T. Durham and I. M. Herman, "Microvascular modifications in diabetic retinopathy," Curr. Diabetes Rep. **11**(4), 253–264 (2011).
37. A. K. Dadzie, D. Le, M. Abtahi, *et al.*, "OCTA-ReVA: an open-source toolbox for comprehensive retinal vessel feature analysis in optical coherence tomography angiography," Github, 2024, https://github.com/fiifijackson/OCTA-ReVA.